

Growth, Characterization and Physical Properties of High-Quality Large Single Crystals of $\text{Bi}_2(\text{Sr}_{2-x}\text{La}_x)\text{CuO}_{6+\delta}$ High Temperature Superconductors

Jianqiao Meng, Guodong Liu, Wentao Zhang, Lin Zhao, Haiyun Liu, Wei Lu, Xiaoli Dong and X. J. Zhou*

National Laboratory for Superconductivity, Beijing National Laboratory for Condensed Matter Physics, Institute of Physics, Chinese Academy of Sciences, Beijing 100190, China

E-mail: XJZhou@aphy.iphy.ac.cn

Abstract.

High quality large $\text{Bi}_2(\text{Sr}_{2-x}\text{La}_x)\text{CuO}_{6+\delta}$ (La-Bi2201) single crystals have been successfully grown by the traveling solvent floating zone technique. The samples are characterized by compositional and structural analyzes and their physical properties are investigated by magnetic susceptibility and resistivity measurements. Superconducting samples with sharp superconducting transitions are obtained covering a wide range of doping from overdoped ($x < 0.40$), optimally-doped ($x \sim 0.40$), underdoped ($0.40 < x < 0.84$) to heavily underdoped without superconducting transition ($x > 0.84$). Crystals as large as $\sim 40 \times 2.0 \times 1 \text{ mm}^3$ are obtained for $x = 0.73$. Sharp superconducting transition with a width less than 2 K and nearly perfect Meissner signal of superconductivity are achieved for $x = 0.40$. The availability of the La-Bi2201 single crystals will provide an ideal system to study the physical properties, electronic structure and mechanism of high temperature superconductivity.

1. Introduction

The physical properties of the copper–oxide (cuprate) superconductors are characterized by the unusually high critical temperature (T_c), the unusual superconducting state with predominantly d -wave pairing [1], and exotic normal state where a pseudogap is present in the underdoped and optimally doped regions[2]. Since the conventional Fermi liquid theory for metals[3] and the BCS theory for conventional superconductivity[4] can not be directly applicable to the cuprate superconductors, new theories have to be developed. Nearly twenty years after its first discovery[5], the mechanism of high-temperature superconductivity in cuprates remains an outstanding issue in condensed matter physics[6, 7]. Critical experiments such as angle-resolved photoemission spectroscopy(ARPES)[8], neutron scattering[9], Scanning tunneling microscopy/spectroscopy(STM/STS)[10] and etc. are necessary in stimulating, checking and developing new theories. High quality single crystal samples are crucial for carrying out these experiments. In some experiments, large size and large quantity of single crystals are needed such as in neutron scattering measurements.

The $\text{Bi}_2\text{Sr}_2\text{CuO}_6$ (Bi2201) superconductor is an ideal system in investigating high temperature superconductivity in cuprates[11]. First, it has a layered structure which can be easily cleaved to get a clean and smooth surface, which is necessary for experiments like ARPES and STM/STS. Second, it has simple single-layered crystallographic structure with one CuO_2 plane within two adjacent block layers, this gives single band and single Fermi surface sheet, avoiding possible complications from two-layered or multi-layered compounds such as bilayer splitting in double-layered $\text{Bi}_2\text{Sr}_2\text{CaCu}_2\text{O}_8$ (Bi2212)[12]. Third, by partially replacing Sr^{2+} with some rare earth ions (R^{3+}) in $\text{Bi}_2(\text{Sr}_{2-x}\text{R}_x)\text{CuO}_{6+\delta}$, the critical temperature of Bi2201 can be increased from around ~ 9 K for the pristine Bi2201[13, 14] to nearly 38 K for $\text{R}=\text{La}$ (lanthanum)[15, 16, 17]. The relatively lower critical temperature, compared with that of Bi2212 and $\text{YBa}_2\text{Cu}_3\text{O}_{7-\delta}$ with a maximum T_c higher than 90 K, is beneficial in investigating normal state properties while suppressing possible thermal broadening caused by high temperature. Fourth, by substituting Sr^{2+} with rare-earth (R^{3+}) which introduces electrons, together with oxygen annealing, the doping level of the samples can be varied over a wide range. In the case of La-doped Bi2201, various doping levels from underdoped, optimally doped and overdoped samples, and even heavily underdoped non-superconducting samples can be obtained[13, 14, 18, 19, 20]. This large doping range is very important for addressing many important issues such as metal–insulator transition, non-superconducting–superconductor transition and other doping evolution of the electronic structure and physical properties of cuprate superconductors.

There have been a few attempts in growing $\text{Bi}_2(\text{Sr}_{2-x}\text{La}_x)\text{CuO}_{6+\delta}$ (abbreviated as La-Bi2201 hereafter) single crystals[21, 22, 23, 24, 25]. While the usual self–flux method[21, 22] is possible, the traveling solvent floating zone method is advantageous in getting large size, better control of the composition and high quality by avoiding possible contaminations from crucibles[23, 24, 25]. In this paper, we report growth

Table 1. Nominal and measured composition, growth conditions, c -axis lattice constant and $T_{c,onset}$ of $\text{Bi}_2(\text{Sr}_{2-x}\text{La}_x)\text{CuO}_{6+\delta}$ single crystals

Nominal Composition	Measured Composition	Growth Rate(mm/h)	Growth Atmosphere	$c(\text{\AA})$	$T_{c,onset}$ (K)
$\text{Bi}_2\text{Sr}_{1.75}\text{La}_{0.25}\text{CuO}_{6+\delta}$	$\text{Bi}_2\text{Sr}_{1.68}\text{La}_{0.30}\text{CuO}_{6+\delta}$	0.5	100 cc/min Air flow	24.519	28
$\text{Bi}_2\text{Sr}_{1.63}\text{La}_{0.37}\text{CuO}_{6+\delta}$	$\text{Bi}_2\text{Sr}_{1.72}\text{La}_{0.36}\text{CuO}_{6+\delta}$	0.5	100 cc/min O_2 flow	24.445	30
$\text{Bi}_2\text{Sr}_{1.60}\text{La}_{0.40}\text{CuO}_{6+\delta}$	$\text{Bi}_2\text{Sr}_{1.64}\text{La}_{0.39}\text{CuO}_{6+\delta}$	0.5	100 cc/min O_2 flow	24.392	32
$\text{Bi}_2\text{Sr}_{1.40}\text{La}_{0.60}\text{CuO}_{6+\delta}$	$\text{Bi}_2\text{Sr}_{1.31}\text{La}_{0.64}\text{CuO}_{6+\delta}$	0.5	50 cc/min O_2 flow	24.222	24.5
$\text{Bi}_2\text{Sr}_{1.30}\text{La}_{0.70}\text{CuO}_{6+\delta}$	$\text{Bi}_2\text{Sr}_{1.28}\text{La}_{0.71}\text{CuO}_{6+\delta}$	0.5	20 cc/min O_2 flow	24.171	20
$\text{Bi}_2\text{Sr}_{1.27}\text{La}_{0.73}\text{CuO}_{6+\delta}$	$\text{Bi}_2\text{Sr}_{1.29}\text{La}_{0.75}\text{CuO}_{6+\delta}$	0.5	20 cc/min O_2	24.148	18
$\text{Bi}_2\text{Sr}_{1.16}\text{La}_{0.84}\text{CuO}_{6+\delta}$	$\text{Bi}_2\text{Sr}_{1.10}\text{La}_{0.97}\text{CuO}_{6+\delta}$	0.5	20 cc/min O_2	24.052	ns

of high quality large-size La-Bi2201 single crystals by traveling solvent floating zone method. The single crystals we have grown cover a wide doping range from overdoped ($x=0.25$), to optimally doped ($x=0.40$), to underdoped (x larger than 0.40) all the way to heavily underdoped without superconducting transition ($x=0.84$). The crystal size we have obtained is up to 3~4cm long. The superconducting samples show a sharp superconducting transition and nearly a perfect Meissner shielding of superconductivity. The successful growth of these single crystal will be very helpful in carrying out some critical experiments to investigate high temperature cuprate superconductors.

2. Experiment method

The $\text{Bi}_2(\text{Sr}_{2-x}\text{La}_x)\text{CuO}_{6+\delta}$ single crystals are grown by traveling solvent floating zone method using an infrared radiation furnace (*Crystal Systems Inc.*) equipped with four 300 W halogen lamps. The high temperature gradient required to stabilize the molten zone can be achieved by ellipsoidal mirrors that focus the image of the four lamps at a common position. The temperature of the molten zone can be controlled precisely by adjusting the output power. The crystal growth was carried out in an enclosed quartz tube where the growth atmosphere can be controlled.

Feed rods and seed rods are first prepared by conventional solid-state reaction method before growing single crystals. Starting materials of Bi_2O_3 , SrCO_3 , La_2O_3 (pre-heated for 5 hours at 860°C to remove the adsorbed water and CO_2) and CuO with 99.99% purity were weighed according to the chemical formula $\text{Bi}_2(\text{Sr}_{2-x}\text{La}_x)\text{CuO}_{6+\delta}$ with different x and mixed in an agate mortar for about 8 hours. The mixed powder was calcined at 780°C for 24 hours and the calcined product was reground into fine powders. This calcination and grinding procedure was repeated for four times to ensure a complete reaction and homogeneity of the calcined powders. The calcined powder was pressed into a cylindrical rod of 7 mm in diameter and 120 mm in length under a hydrostatic pressure of ~ 70 MPa, followed by sintering in a vertical molisili furnace at 870°C for 48 h in air. The sintered rod was then pre-melted in the floating zone furnace at a traveling velocity of 25~30 mm/hour to obtain a dense feed rod with ~ 6 mm in diameter and ~ 120 mm in length. The pre-melting is a crucial step in achieving a stable molten zone during the crystal growth because it may prevent the molten zone from



Figure 1. Photos of $\text{Bi}_2(\text{Sr}_{2-x}\text{La}_x)\text{CuO}_{6+\delta}$ single crystals cleaved from as-grown ingots with various nominal compositions: $x = 0.25, 0.37, 0.40, 0.60, 0.70, 0.73$ and 0.84 . Some crystals with large x can reach 3~4 cm in length.

penetrating into the feed rod. An ingot about 1.5 cm long cut from the pre-melted feed rod was used as a seed rod.

The crystal growth involves many trials to optimize growing conditions, including the power used, growth rate, rotation rates of feed rod and the seed rod, and growing atmosphere. These conditions vary for different compositions. Table 1 lists La-Bi2201 crystals with different compositions, their growth conditions, and the structural and superconducting properties. Some key parameters to obtain high-quality large La-Bi2201 single crystals are briefly described below:

(1). The output power is in principle dictated by the melting point of the feed rod. In practice it can be estimated during the pre-melting process. An optimized output power can be achieved by fine-tuning within a narrow range which gives rise to an appropriate molten zone that can stay stable during the entire growth process.

(2). The growth rate is determined by the atomic diffusion kinetics during the crystal growing process which may vary significantly among different materials. The stability of the molten zone and the crystal size are other factors to take into account. For La-Bi2201, when a lower growth rate (<0.45 mm/hour) was used, the molten zone tends to become unstable causing frequent collapse of the zone. When a higher growth rate (>0.8 mm/hour) is used, although the molten zone gets more stable, the size of the single crystals size gets smaller. As a compromise, a growth rates of 0.5 mm/hour was used for growing La-Bi2201 single crystals.

(3). The feed rod and the seed rod both rotate in the opposite direction in order to ensure efficient mixing and uniform temperature distribution in the molten zone. A 30/20 rpm rate was used for feed rod (upper shaft)/seed rod (lower shaft) in growing La-Bi2201. The upper shaft rotates faster to make the molten zone more homogenous,

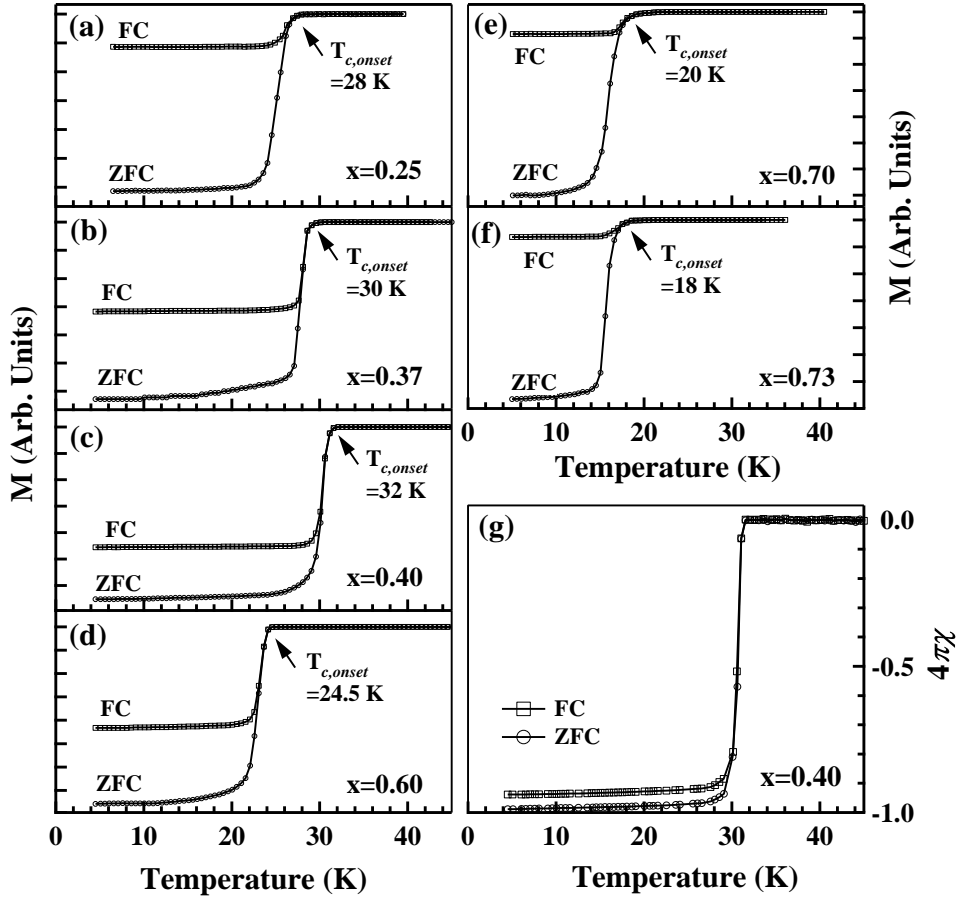


Figure 3. Temperature dependence of magnetization of La-Bi2201 single crystals measured using under a magnetic field of 1 Oe: (a) $x = 0.25$, (b) $x = 0.37$, (c) $x = 0.40$, (d) $x = 0.60$, (e) $x = 0.70$, (f) $x = 0.73$. (g) Magnetic susceptibility χ for another well-annealed $x = 0.40$ single crystal.

Fig.1 shows some typical La-Bi2201 single crystals with different La concentration that were cleaved from the top of the as-grown ingots. We note that for the initial part of the ingot (0~3 cm), because the growing conditions were not yet optimized and stable, the crystal size is usually small with lower quality. Large high-quality crystals are obtained in the final part of the ingot when the growth process is optimized and stable.

The as-grown single crystals were post-annealed in flowing oxygen at different temperatures ($450^\circ\text{C} \sim 700^\circ\text{C}$) for 2 ~ 12 days to adjust the carrier concentration and make the samples uniform. During the annealing process, the crystals were embedded in the sintered powders with the same composition to avoid evaporation of some constituents. After annealing, the samples were quenched in liquid nitrogen. Compared with the as-grown crystals, such an annealing process has a weak effect on T_c value for most of the compositions, except for $x=0.84$ which, when as-grown, is not superconducting down to 2 K, but can become superconducting with a T_c up to 10 K after annealing in oxygen for sufficiently long time.

3. Results and discussion

As shown in Fig. 1, large La-Bi2201 single crystals with various compositions, x , have been successfully grown. For the composition ($x = 0.73$), single crystal as long as ~ 40 mm has been obtained. It is found that the crystal size relies closely on the starting composition. The viscosity of La-Bi2201 increases with increasing La concentration, x , which makes the molten zone more stable. This is probably why it is easier to get large single crystals at high La concentration (Fig. 1).

After post-annealing, the single crystals were characterized in the composition and crystal structure. The superconducting properties were investigated by both resistivity and magnetic susceptibility measurements.

3.1. Compositional analysis

The chemical composition of the La-Bi2201 crystals was determined by the induction-coupled plasma atomic emission spectroscopy (ICP-AES). The results are given in Table 1. The actual composition of the grown single crystals is very close to their nominal composition for $x=0.37\sim 0.73$ while the deviation of the $x=0.25$ and 0.84 samples is slightly larger. Overall, this indicates that the sample homogeneity and composition are well controlled during the entire single crystal growth process.

3.2. Structure characterization

The structure and quality of the single crystals are characterized by X-ray diffraction (XRD) using a rotating anode X-ray diffractometer with Cu K_α radiation ($\lambda=1.5418$ Å). The experiments were carried out under θ - 2θ scan mode with incident ray along the c -axis of the single crystal, and the continuous scanning range of 2θ is from 5° to 75° . Fig. 2 shows XRD patterns for the La-Bi2201 with various compositions $x = 0.25, 0.37, 0.40, 0.60, 0.70, 0.73$ and 0.84 . All the observed peaks can be indexed to the Bi2201 structure, indicating a pure single-phase of the obtained single crystal. The peaks are sharp, as exemplified from the (008) peaks in the inset of Fig. 2 which has a width of $0.08\sim 0.09$ degree (Full Width at Half Maximum), indicating high crystallinity and high orientation of the single crystals.

The c -axis lattice parameters of the single crystals undergoes a systematic change with the La content x , as shown by the peak position shift in the inset of Fig. 2. The c -axis lattice constant is calculated from XRD data[26], as listed in Table 1 and shown in Fig. 5(b). It decreases with increasing La doping which is consistent with the fact that La^{3+} has a smaller ionic radius than Sr^{2+} . The c -axis lattice constant shows a linear relation with the nominal La concentration x which can be approximated as $c(\text{nm})=2.472-0.0795x$. In Fig. 5(b), we also plot the data from other groups[19, 20, 23] which show a good agreement with each other.

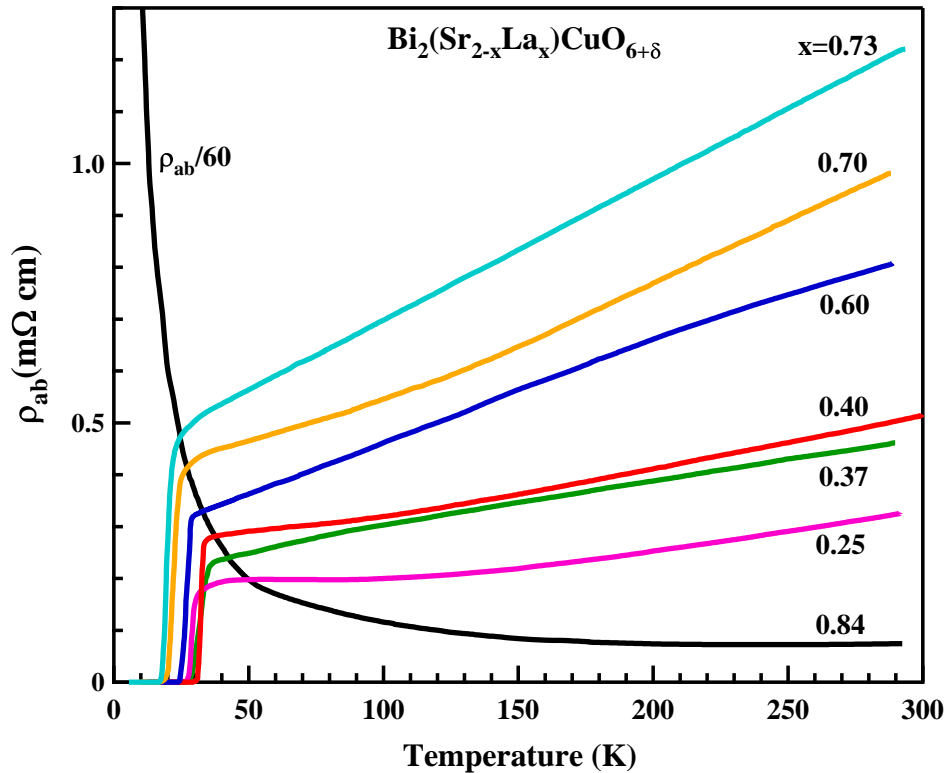


Figure 4. Temperature dependence of in-plane resistivity ρ_{ab} of the La-Bi2201 crystals for various nominal La content (x)

3.3. Superconductivity

The superconducting transition temperature of the annealed La-Bi2201 crystals is determined by both magnetization (Fig. 3) and resistivity (Fig. 4) measurements. Fig.3 shows the temperature dependence of DC magnetization for La-Bi2201 single crystals with various La content x , measured using a Quantum Design MPMS XL-1 system with a low magnetic field of 1 Oe. The crystals with $x=0.25 \sim 0.75$ show clear superconducting transition while the as-grown $x=0.84$ sample is non-superconducting down to 2 K. The superconducting transition temperature (T_c), defined by the onset of a diamagnetic signal, increases with x first, reaching a maximum $T_{c,onset}=32$ K near $x=0.4$, and decreases with further increase of x . Since the substitution of Sr^{2+} with La^{3+} is expected to introduce electrons into the samples and it is well-known that Bi2201 is a hole-doped system, increasing La concentration would result in a decrease of the hole concentration. Therefore, samples with x less than 0.4 are expected to be over-doped, $x \sim 0.4$ is optimally-doped while x larger than 0.4 is under-doped.

It is also clear from Fig. 3 that the prepared single crystals show sharp superconducting transition with a transition width $\Delta T_c=1 \sim 3$ K (10%~90% standard). In order to further investigate the quality of the superconducting samples, we choose a well-annealed $x = 0.40$ sample for quantitative investigation. Its magnetic susceptibility has been carefully calculated by considering its volume and correcting

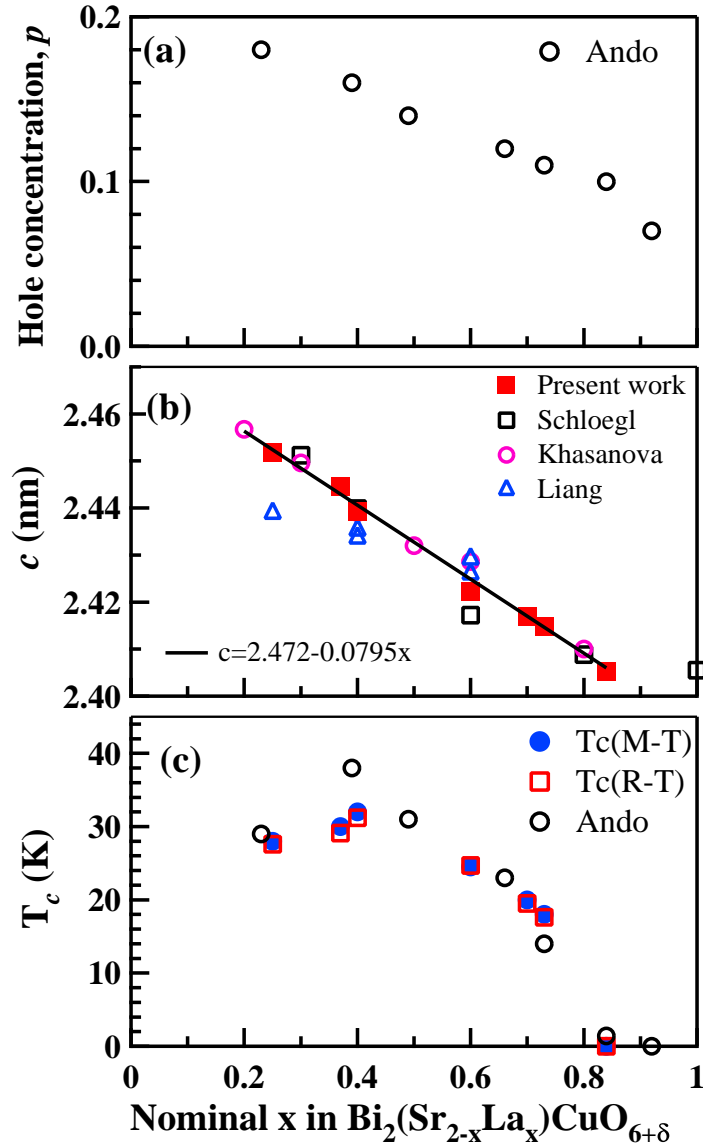


Figure 5. (a) Relation of the hole concentration p as estimated from thermopower measurements with the nominal La content by Ono et al.[24].(b) Dependence of the c -axis lattice constant on the nominal La concentration (x). Data from other groups are also included[18, 19, 20, 23, 27, 28]. The solid line is fitted to our measured data.(c) T_c as a function of nominal La content (x). Data by Ono et al. are also plotted[24].

the demagnetization factor by considering its shape. As shown in Fig. 3(g), this sample shows a sharp superconducting transition at 31.5 K with a width of ~ 1 K. Its 100% shielding (zero-field-cooled, ZFC) signal indicates there exists little macroscopic inhomogeneity or weak links. Its extremely high Meissner signal ($\sim 95\%$, field-cooled FC) implies that this sample is nearly free of pinning disorders. Nearly complete shielding and Meissner effects demonstrate the high quality of this crystal.

Fig. 4 shows the temperature dependence of in-plane resistivity ρ_{ab} for all the grown La-Bi2201 single crystals with various compositions. The in-plane resistivity

was measured using the standard four-probe method. Gold lead wires were attached to the contact pads using silver epoxy and then were annealed at 400°C. Consistent with DC magnetic measurements (Fig. 3), the samples with $x=0.25\sim 0.75$ show clear superconducting transition while the $x=0.84$ sample shows an insulating behavior. The superconducting transition temperature increases with x first, reaching a maximum of 31 K (zero resistance) at $x=0.40$, and getting smaller with further increase of x . While there may be a relatively large uncertainty in the absolute value of resistivity, the overall trend is that the magnitude of ρ_{ab} increases with increasing La content from $x = 0.25$ to 0.84, consistent with previous measurements[18, 27, 28].

Fig. 5 summaries the c -axis lattice (Fig. 5(b)), superconducting transition temperature (Fig. 5(c)) of the La–Bi2201 single crystals as a function of La concentration x . Data from other groups[18, 19, 20, 23, 27, 28] are also included for comparison and completeness. Particularly, the hole concentration estimated from thermopower measurements by Ono and Ando[24] is plotted in Fig. 5(a). These results provide useful information in corresponding the carrier concentration, c -axis lattice constant and the superconducting transition temperature in La–Bi2201 system.

In summary, high-quality and large La–Bi2201 single crystals with wide range of compositions have been successfully prepared by traveling solvent floating zone method. It will provide an ideal candidate for investigating the electronic structure[29] and physical properties, and superconductivity mechanism of high temperature superconductors.

Acknowledgments

This work is supported by the NSFC (Project No: 10525417, 10734120, 10874211), the MOST of China (973 project No: 2006CB601002 and 2006CB921302), and CAS (Projects ITSNEM).

References

- [1] See. e.g. Tsuei. C. C and J. R. Kirtley 2000 Rev. Mod. Phys. **72** 969.
- [2] T. Timusk and B. Statt 1999 Rep. Prog. Phys **62** 61.
- [3] L. D. Landau, Zh. Eksp. Tear. Fiz. **30**, 1058(1956) [Sov. Phys.-JETP **3**, 920 (1957)]; L. D. Landau, Zh. Eksp. Tear. Fiz. **32** 59 (1957) [Sov. Phys.-JETP **5** 101 (1957)].
- [4] J. Bardeen, L. N. Cooper and J. R. Schrieffer 1957 Phys. Rev **108** 1175.
- [5] J. G. Bednorz and K. A. Muller 1986 Z. Phys. B **64** 189.
- [6] J. Orenstein and A. J. Millis 2000 Science **288** 468.
- [7] D. A. Bonn 2006 Nature Physics **2** 159.
- [8] A. Damascelli, Z. Hussain and Z.-X. Shen 2003 Rev. Mod. Phys **75** 473; J. C. Campuzano, M. R. Norman and M. Randeria, in The Physics of Superconductors, Vol. 2: Photoemission in the High- T_c Superconductors, chapter 17, edited by K. H. Bennemann and J. B. Ketterson, (Springer, 2004); X. J. Zhou, T. Cuk, T. Devereaux, N. Nagaosa, and Z. -X. Shen, in Handbook of High-Temperature Superconductivity: Theory and Experiment, Chapter 3, edited by J. R. Schrieffer, (Springer, 2007).
- [9] J. M. Tranquada, in Handbook of High-Temperature Superconductivity: Theory and Experiment, chapter 6, edited by J. R. Schrieffer, (Springer, 2007).

- [10] Φ ystein Fischer, Martin Kugler, Ivan Maggio-Aprile, Christophe Berthod and Christoph Renner 2007 Rev. Mod. Phys **79** 353.
- [11] A. Maeda, M. Hase, I. Tsukada, K. Noda, S. Takebayashi, K. Uchinokura 1990 Phys. Rev. B **41** 6418.
- [12] D. L. Feng, N. P. Armitage, D. H. Lu, A. Damascelli, J. P. Hu, P. Bogdanov, A. Lanzara, F. Ronning, K. M. Shen, H. Eisaki, C. Kim, and Z.-X. Shen 2001 Phys. Rev. Lett **86** 5550; Y.-D. Chuang, A. D. Gromko, A. Fedorov, Y. Aiura, K. Oka, Yoichi Ando, H. Eisaki, S. I. Uchida, and D. S. Dessau 2001 Phys. Rev. Lett. **87** 117002; P. V. Bogdanov, A. Lanzara, X. J. Zhou, S. A. Kellar, D. L. Feng, E. D. Lu, H. Eisaki, J.-I. Shimoyama, K. Kishio, Z. Hussain, and Z. X. Shen 2001 Phys. Rev. B **64** 180505.
- [13] B. Liang, A. Maljuk, C. T. Lin 2001 Physica C **361** 156.
- [14] Huiqian Luo, Lei Fang, Gang Mu, Hai-Hu Wen 2007 Journal of Crystal Growth **305** 222.
- [15] P. V. P. S. S. Sastry and A. R. West 1994 Physica C **225** 173.
- [16] H. Eisaki, N. Kaneko, D. L. Feng, A. Damascelli, P. K. Mang, K. M. Shen, Z.-X. Shen and M. Greven 2004 Phys. Rev. B **69** 064512.
- [17] Y. Ando, A. N. Lavrov, S. Komiya, K. Segawa and X.F. Sun 2001 Phys. Rev. Lett **87** 17001.
- [18] Y. Ando and T. Murayama 1999 Phys. Rev. B **60** 6991.
- [19] A. E. Schlöbl, J. J. Neumeier, J. Diederichs, C. Allgeier and J. S. Schilling 1993 Physica C, **216** 417.
- [20] N. R. Khasanova and E. V. Antipov 1995 Physica C, **246** 241.
- [21] N. L. Wang, B. Buschinger, C. Geibel, F. Steglich 1996 Phys. Rev. B **54** 7449.
- [22] W.L. Yang, H.H. Wen, Y.M. Ni, J.W. Xiong, H. Chen, C. Dong, F. Wu, Y.L. Qin, Z.X. Zhao 1998 Physica C **308** 294.
- [23] B. Liang, C. T. Lin 2004 Journal of Crystal Growth **267** 510.
- [24] S. Ono, Y. Ando 2003 Phys. Rev. B **67** 104512.
- [25] Huiqian Luo, Peng Cheng, Lei Fang and Hai-Hu Wen 2008 Supercond. Sci. Technol **21** 125024.
- [26] C. Dong, F. Wu, H. Chen 1999 J. Appl. Crystallogr. **32** 850; C. Dong, H. Chen, F. Wu 1999 J. Appl. Crystallogr. **32** 168; C. Dong 1999 J. Appl. Crystallogr. **32** 838.
- [27] S. Ono, Y. Ando, T. Murayama, F. F. Balakirev, J. B. Betts, and G. S. Boebinger 2000, Phys. Rev. Lett. **85** 638.
- [28] Y. Ando, Y. Hanaki, S. Ono, T. Murayama, K. Segawa, N. Miyamoto, and S. Komiya 2001 Phys. Rev. B **61** 14956.
- [29] Jianqiao Meng, Wentao Zhang, Guodong Liu, Lin Zhao, Haiyun Liu, Xiaowen Jia, Xiaoli Dong, Wei Lu, Guiling Wang, Hongbo Zhang, Yong Zhou, Yong Zhu, Xiaoyang Wang, Zhongxian Zhao, Zuyan Xu, Chuangtian Chen, X. J. Zhou 2009 Phys. Rev. B **79** 024514.